Arch. Metall. Mater. **64** (2019), 2, 707-713

DOI: 10.24425/amm.2019.127602

A. MUNIS*, MAOSHENG ZHENG*#, J.I. AKHTER**, M. AHMAD***

CHARACTERIZATION OF BONDED ZONE AND EVALUATION OF CRACKING IN VACUUM BRAZED ZIRCALOY-4 AND STAINLESS STEEL-316L JOINT

Brazing of two dissimilar structural materials; Zircaloy-4 and SS-316L was performed at 900°C under high vacuum conditions. The metallic glass ribbons ($Zr_{55}Cu_{30}Al_{10}Ni_2Fe_3$-at. %) of 30 μm thickness, were used as an interlayer. The bonded region was characterized by scanning electron microscope (SEM), energy dispersive spectroscope (EDS) and microhardness testing. The metallurgical bond formation was due to compositional changes in the molten interlayer and later on its subsequent solidification. Assessment of the bonded zone (BZ) revealed three distinct regions (Region-I, Region-II and Region-III). Diffusion transformation was observed in Region-I and Region-III which were interface with base alloys SS-316L and Zircaloy-4 respectively. However, Region-II at the middle of the BZ was composed of isothermally and athermally solidified portions. The highest values of Microhardness were observed in Region-III which was due to the presence of hard phases. Moreover, a crack parallel to BZ was observed in Region-III and was attributed to differential contraction of base alloys during cooling. Maximum shear stress acting on the BZ was calculated and correlated to the brittle phase cracking.

Keywords: Bonded Zone (BZ), Intermetallics, Vacuum Brazing, Interlayer, Cracking

1. Introduction

The joining of Zirconium alloy to Stainless Steel (SS) is frequently required in many nuclear applications, like in-core/ out-of-core components. In pressurized heavy water reactors (PHWR) some examples of such joints are pressure tube/end fittings, CALANDRIA tube/ tube sheet of CALANDRIA vessel and temperature monitoring assemblies [1]. The conventional fusion welding for bonding these materials is undesirable because the coefficient of thermal expansions and fusion temperatures of both alloys differ largely [2-4]. Welding of dissimilar material by electron/laser beam welding is another option. This technique can produce better weld microstructure as compared to the conventional welding techniques. The success of laser/electron beam welding lies mainly in the local melting and fast cooling during the course of welding process. Electron beam welding of Zircaloy-4 and SS-304 shows reduction in heat affected zone (HAZ) and diffusion zone (DZ) along with low density of undesired phases [5]. However, thickness of the samples to be welded by this process is limited.

Different attempts have been made to weld dissimilar materials especially Zirconium alloys and Stainless Steels through diffusion bonding with varying degree of success. Shaaban et al. [6] have studied diffusion bonding between Zircaloy-4 and SS-304, and reported formation of brittle intermetallic phases in DZ. Many researchers have introduced diffusion barriers in the form of interlayer to minimize or to prevent the formation of intermetallic compounds in the DZ. Shaaban et al. [7] used Fe interlayer; Wayman et al. [8] used Pt., Ahmed et al. [9] introduced Ta interlayer, while Kale et al. [10] tried both Ti and Fe as diffusion barrier to restrict the formation of intermetallic phases in DZ.

The use of amorphous interlayer for vacuum brazing makes the joining process a viable industrial trend [11]. Bajgholi et al. [12] used STEMET 1228 amorphous Ti base filler as an interlayer for vacuum brazing of Zr-Nb2.5 and SS-321. However, the use of Zirconium base amorphous interlayer for vacuum brazing of Zircaloy-4 and SS-316L is still rare. $Zr_{55}Cu_{30}Al_{10}Ni_2Fe_3$-at % amorphous alloy has low melting point (857°C) [13] and it's constituents also make deep eutectics with base alloys. These properties make it a suitable candidate to be used as an interlayer. The present study primarily investigates the possibilities of bonding at different vacuum levels and the different phases formed in the bonded zone (BZ). Furthermore, an attempt is also made to calculate the stress acting on the BZ. System under study is a joint between dissimilar materials having different coefficient of thermal expansion. Therefore, during cooling the differential contraction of the bonded metals exerts a shear stress on the BZ and this shear stress depends on the thickness of the BZ. The bonded assembly of Zircaloy-4 and SS-316L is represented as

* NORTHWEST UNIVERSITY, SCHOOL OF CHEMICAL ENGINEERING, INSTITUTE OF ENERGY TRANSMISSION TECHNOLOGY AND APPLICATION, XI'AN, 710069, CHINA
** PINSAT, PRESTON UNIVERSITY, ISLAMABAD, PAKISTAN
*** PHYSICS DIVISION, DIRECTORATE OF SCIENCE, PINSTECH, P.O. NILORE, ISLAMABAD, PAKISTAN
# Corresponding author: mszhengok@aliyun.com

two elastic layers without bending and stress analysis model proposed by chen et al [14] is employed for the calculation of shear stresses acting on the BZ. This proposed model inherits the Volkerson's lap joint analysis in addition to the thermal considerations [15].

2. Experimental procedure

Nominal compositions of base alloys used in this study are given in Table 1. Samples of 200 mm × 100 mm × 50 mm were cut from sheets of SS-316L and Zircaloy-4 with the help of slow cutter. The surfaces to be joined were grounded to 1200 grit finish, degreased with alcohol and rinsed with distilled water. Ribbons of $Zr_{55}Cu_{30}Al_{10}Ni_2Fe_3$ amorphous alloy having thickness 30 μm and width 3 mm were used as interlayer. After holding together with Platinum-Rhodium wire, the samples were then pressed in a vice machine for 24 hours. The purpose of pressing samples in the vice machine was to introduce plastic deformation to the surfaces and to break the surface oxide layer. Four samples were prepared and treated under different vacuum conditions, as given in Table 2.

TABLE 1

Nominal composition of base alloys

Alloy	Element (wt %)							
	Sn	Cr	Ni	Mo	C	Mn	Fe	Zr
Zircaloy-4	1.52	01	<0.005	—	0.002	—	0.2	Balance
SS-316L	—	17	12	2.5	0.08	2	65	—

TABLE 2

Experimental Conditions

Sample No.	Heating Rate (°C/min)	Brazing Temperature (°C)	Holding Time (Hrs)	Cooling Condition	Vacuum (bar)	Bonding
01	—	900	02	Air	No	No
02	—	900	03	Furnace cool	4×10^{-1}	No
03	—	900	03	Furnace cool	4×10^{-3}	No
04	10	900	03	Furnace cool	5×10^{-6}	Bonded

First brazing experiment was performed in a muffle furnace with uncontrolled environment. The sample was preheated at 300°C on Alumina boat and then inserted in the furnace. The furnace was maintained at brazing temperature of 900°C and sample was treated for 2 hours. In the second and third experiments samples were loaded separately in the quartz tubes and then tubes were evacuated to vacuum 4×10^{-1} bar and 4×10^{-3} bar, respectively. The bonding temperature 900°C was stabilized before inserting the tubes in the furnace. Samples were treated for three hours at bonding temperature. After that samples were furnace cooled and vacuum was monitored and maintained throughout heating and cooling cycle. The sample no.4 was brazed at same temperature and time however the vacuum level was maintained at 5×10^{-6} bar during fourth experiment. After cooling to ambient temperature all samples were examined visually. For scanning microscope analysis (SEM) the bonded sample was mounted, wet grounded down to 3000 grit and polished with diamond paste. After polishing, the surface was degreased with alcohol and rinsed with distilled water. In order to reveal the microstructure the polished and cleaned surface was etched. The etchant used have the following constituents H_2O_2 : HNO_3 : HF with 50 : 47 : 3 volume ratio respectively. Etching was done by swabbing the surface. The hardness testing of BZ was carried out by using Vickers Micro Hardness Tester. The measurements were taken from three different locations and at least three readings were recorded and values are reported in Table 3.

3. Results and discussions

The temperature, holding time and environment play a decisive role in brazing process. Brazing temperature is usually selected by keeping in view that the deep eutectics of the base alloys and melting range of interlayer overlap. In order to study the effect of environment on brazing process, samples were treated at different vacuum levels. During first attempt of brazing, severe oxidation was observed on base alloys surfaces and also on interlayer thus no bonding was resulted. Similarly, in second and third attempts, samples were treated in rough vacuum of 4×10^{-1} bar and 4×10^{-3} bar for 3 hours respectively. The bond formation was unsuccessful between zircaloy-4 and ss-316L in both cases as well. However, melting and adherence of interlayer with base alloys was observed in the brazing

TABLE 3

Microhardness (VHN) Values across the bonded zone (BZ)

Location of BZ	VHN (avg.) Load: 25g, Loading Time: 15 sec									Average
	Location (a)			Location(b)			Location(c)			
	i	ii	iii	i	ii	iii	i	ii	iii	
SS-316 L (Base Alloy)	157	162	161	159	150	165	155	156	156	158
Region-I	183	195	204	182	198	198	200	186	180	191
Region-II	Not Possible									
Region-III	436	421	430	418	440	440	414	426	426	428
Ziraloy-4 (Base Alloy)	146	152	154	150	148	148	144	150	146	149

experiment conducted at 4×10^{-3} bar vacuum see Fig. 1. Black patches were also observed on the adherent interlayer and were attribute of oxidation. Therefore, to avoid oxidation the vacuum level was increased to 5×10^{-6} bar in fourth experiment. As a result a metallurgical bond was formed between Zircaloy-4 and SS-316L.

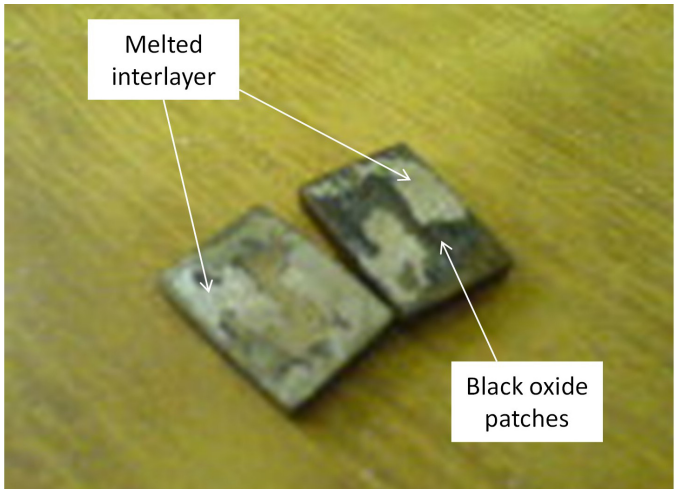

Fig. 1. Sample No. 3 treated in vacuum of 4×10^{-3} bar for 3 hours

The SEM image of BZ and base metal interfaces was shown in Fig. 2(a). The width of the BZ was measured to be ~225 µm and it was found to be larger in comparison to the thickness of the interlayer used. It was perceived that at brazing temperature the interlayer was melted and transformed into a molten pool of an alloy. At the brazing temperature the surfaces of base metal reacted with the molten interlayer. In order to maintain the equilibrium at the solid/liquid interface the base metal was dissolved by the molten interlayer which resulted in the widening of the liquid metal pool [16]. Moreover, diffusion of the atoms into the base alloy matrix was also occurred. In this way a larger BZ was formed. Interestingly, no morphological indications of diffusion of solute atoms into the SS-316L matrix were observed. On the other hand, a cracked interface with Zircaloy-4 was observed which may be due to the fragility of some brittle phase present. Higher magnification image of BZ is shown in Fig. 2(b). The figure revealed that BZ was comprised of three morphologically distinct regions. Region-I and region-III were interfacing SS-316L and Zircaloy-4 respectively, while region-II was observed at the middle of BZ. Region-III was found to be the largest and ~155 µm wide in comparison with Region-I and Region-II which were measured ~8 µm, ~62 µm wide respectively. Since, the brazing temperature was well above the melting point (857°C) of interlayer. Therefore, at brazing temperature interlayer was melted and transformed into a liquid metal pool. The interaction of molten interlayer with base alloys interfaces was resulted in dissolution of interfacial surfaces. In this way the chemical composition of molten interlayer was changed. The dissolution of SS-316L introduced Fe, Ni and Cr while Zircaloy-4 contributed Zr and Sn into the liquid pool. The solute atoms of Fe, Ni from SS-316L and Cu from interlayer were diffused rapidly

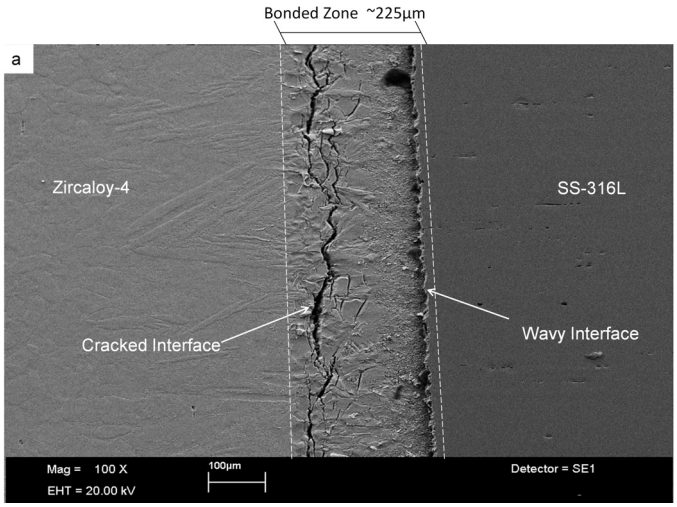

Fig. 2a. Secondary electron image (SEI) of the bonded zone (BZ) made at 900oC in 5×10^{-6} bar pressure

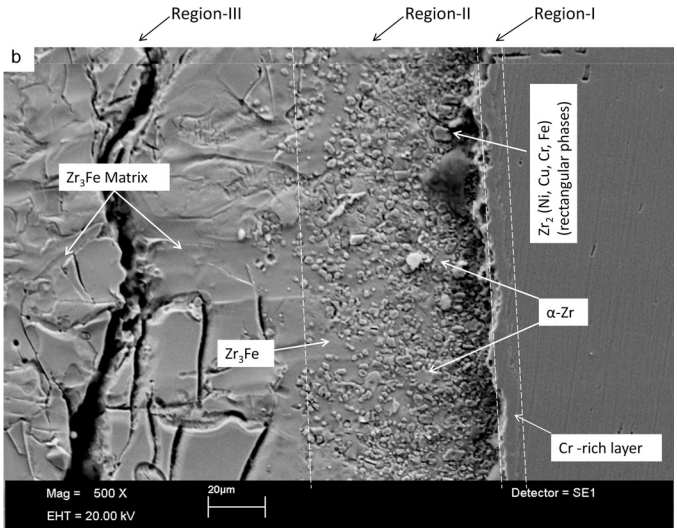

Fig. 2b. High magnification, showing different regions (Region-I, Region-II and Region-III) and crack in BZ

into the molten phase and spread all over the molten pool, as the diffusion of solute atoms is faster in liquid phase [17-18]. The dissolution of interfacial surfaces of base alloys not only changed the chemical composition of molten interlayer but also widen the liquid metal pool.

After the melting of interlayer and widening of liquid phase, an isothermal hold period was emerged during which diffusion of the solute atoms across the solid/liquid interface was occurred. Isothermal solidification of the liquid layer was started at liquid/base alloy interface and advanced towards the center of the joint. Isothermal solidification of the liquid phase is a phenomenon that depends on the compositional changes which increase liquidus temperature. Therefore, a molten pool started to solidify isothermally once it was reached the liquidus temperature. During isothermal solidification, the solute atoms were rejected to the adjacent liquid making it enriched with solute atoms. The remaining liquid enriched with solute atoms was then solidified athermally and a mixture of intermetallic

phases was formed. Since, secondary or intermetallic phases cannot form isothermally because of lack of under-cooling and elemental segregation [19-20].

Fig. 2(c) presented the region-II, it was mainly comprised of multiphase mixture of irregular shaped intermetallics and α-Zr. EDS analysis of region-II showed that it was a Zr rich alloy with 50-70 at. % of Zr. Other than Zirconium, the appreciable amount of Ni, Cu, Fe, Sn and Cr were also observed. The chemical composition of interlayer and Zircaloy-4 showed complete absence of Cr. Therefore, presence of Cr in the region-II was only due to the dissolution of SS-316L interfacial surfaces. Similarly, presence of Sn was attributed to the melting of interfacial surface of Zircaloy-4. The composition and relative proportions of different phases formed in three distinct regions were listed in Table 4. The elemental contents of Zr and other metals in regions-II were near to stoichiometric value of Zr_2 (Ni, Cu, Fe, Cr). In Ni-Zr binary system, maximum solid solubility of Ni in β-Zr is 2.92 at. % at eutectoid temperature (845°C). Therefore, at brazing temperature Ni was dissolved in β-Zr phase and formed a solid solution. However, during cooling process when the temperature of BZ was reached to 845°C. The eutectoid reaction was occurred and Ni impregnated β-Zr was converted into α-Zr and Zr_2Ni [21]. Formation of Zr_3Fe in Region-II was due to the Fe diffusion from the matrix to the surface [22]. Contradictory observations were made by L. Kumar et al. [23] as they concluded that furnace cooling from β-phase field resulted in the formation of Zr_2Fe precipitates, suggesting that the formation of Zr_2Fe and Zr_3Fe phases were competitive processes. However, the precipitation of Zr_3Fe is in well accordance with Zr-Fe binary phase diagram and same was reported by Sawicki et al. [24]. Adjacent to Zr_3Fe Phase, island like phases were observed and found to be α-Zr solid solution of Sn. In order to reveal the location of the α-Zr a backscattered image of the BZ zone was taken see Fig. 2(d). The density of intermetallics was observed to be high in Region-II and decreases away towards the Region-III where Zr_3Fe brittle phase was formed.

Region-I has a wavy interface and high Cr concentration was observed in it see Fig. 2(c). At high temperature and vacuum conditions, the oxide film on the surface of SS-316L was depleted and a concentration gradient was developed between the surface and bulk of alloy. In order to fill up the concentration gradient, Cr atoms from the matrix of the SS-316 L were diffused under the influence of high temperature and formed a layer along the surface. Moreover, Cr rich layer served as a diffusion barrier and prevented the Zr atoms to diffuse into the bulk of SS-316L [25].

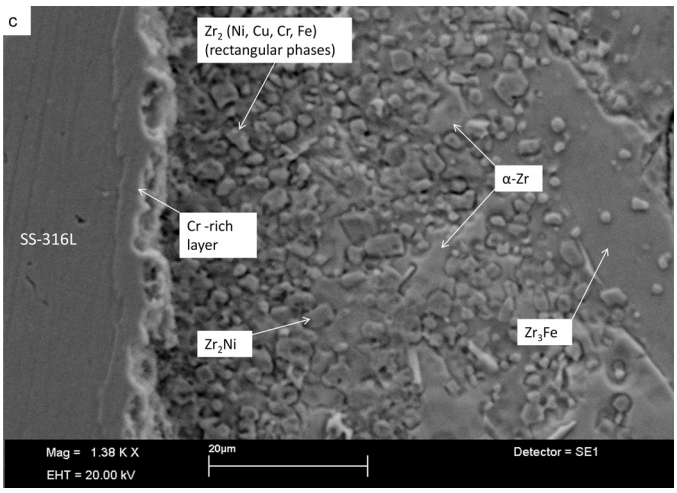

Fig. 2c. SEI image indicating different phases in Region-II and an interface with SS-316L

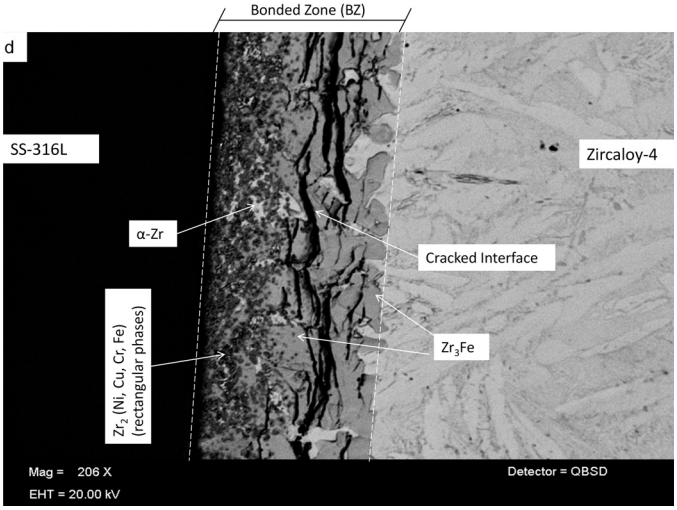

Fig. 2d. Back-scattered image (BSI) showing different phases and crack in BZ

In Region-III, the high diffusivity of Ni and Fe in Zircaloy-4 matrix [26-27] enabled both elements to diffuse further into the Zircaloy-4 matrix at brazing temperature. The solubility of Fe in β-Zr at 900°C is about 6 at. %, therefore, due to the diffusion of Fe into Zrcaloy-4 matrix the β-Zr was converted into Zr_2Fe. Moreover, at brazing temperature β-Zr and Zr_2Fe can coexist [28]. It was believed that before the completion of athermal solidification of remaining solute enriched liquid metal pool.

TABLE 4

Composition of phases observed in bonded zone (BZ)

Regions in BZ	Phases	Relative Proportion	Composition of major elements in at. %					
			Zr	Fe	Ni	Cu	Cr	Sn
Region-I	Cr-Rich Layer	—	5.87	31.94	0.65	2.10	53.85	1.01
Region-II	Zr_2(Ni, Cr, Cu, Fe)	Major	56.48	23.58	3.98	6.74	8.56	—
	Zr_3Fe (Matrix)	Major	62.98	22.16	4.47	4.64	5.14	—
	α-Zr	Minor	70.38	10.05	1.42	1.46	2.74	9.42
Region-III	Zr_3Fe	Major	68.13	20.89	6.24	4.72	—	—

The Fe atoms had already been diffused into the Zircaloy-4 matrix where β-Zr and Zr_2Fe were coexisting. During cooling process, as the temperature was decreased from the brazing temperature. A peritectoid reaction was occurred once the temperature was reached to 885°C and β-Zr + Zr_2Fe were converted to Zr_3Fe. It was therefore, suggested that the formation of Zr_3Fe was due to the diffusion of Fe into Zircaloy-4 matrix from the liquid phase. Microhardness of BZ along with base alloys was recorded and values are reported in Table 3. Microhardness of Region-II was not reported because it was difficult to measure in that region due to high roughness of surface and ambiguous indent shape. Microhardness values of Region-I were found to be in close proximity of hardness of SS-316L. It was because of the Cr-rich layer which restricted the diffusion of the elements having tendency to form hard phases with Fe. The microhardness studies showed that region-III displayed the higher hardness as compare to region-I and base alloys. At SS-316L interface the diffusion of Zr into the matrix was prevented by the Cr-rich layer. On the other hand no such barrier was formed at Zircaloy-4 interface and diffusion of Fe into Zircaloy-4 matrix was occurred. In return, region-III was transformed into brittle and hard Zr_3Fe phase. In order to further evaluate the diffusion profile of different elements across the BZ a compositional line scan was performed and shown in Fig. 3. On traversing from SS-316L through the Region-I the concentration of Cr was increased rapidly. The Cr-rich layer acted as barrier to further diffusion of elements thus as a result no hard intermetallics were formed in Region-I as discussed earlier. .The concentration of Zr was observed to fall drastically across the region-I. This observation was consistent with our claim that Cr rich layer was acted as a barrier against the diffusion of Zr into the SS-316L matrix. The compositional scanning of region-II showed the high concentration of Zr along with Cu, Ni, Cr and Sn. The presence of Cr and Sn also supported the argument that during widening of molten pool the dissolution of SS-316L and Zircaloy-4 was occurred.

Cracking was observed parallel to the center line of the BZ in diffusion transformed Region-III. In transient liquid phase (TLP) bonding process, stages are sequential and cannot occur simultaneously [29-30]. Therefore, it may be inferred that, before the formation of diffusion transformed Regions-I and Region-III, the solidification of Region-II had already been completed. After the completion of solidification of molten phase the BZ was completely in solid state. At this point the Zircaloy-4 interface was impregnated with Fe solute atoms. Upon cooling, peritectoid reaction was occurred at 885°C in solid state and whole Region-III was converted into Zr_3Fe. Formation of different phases; namely, isothermally solidified α-Zr and A-thermally solidified multiphase composite, in region-II has negligible effect on crack formation. Moreover, Transformation of Fe impregnated β-Zr into Zr_3Fe was a solid state reaction and no liquid was present at that time. Therefore, liquation cracking of the Region-III may not be the case. During cooling process, SS-316L was contracted more as compare to Zircaloy-4. Since coefficients of thermal expansion of both alloys differ considerably see Table 5. A shear stress was exerted on BZ due to the differential contraction of base alloys. The shear stress was not uniformly distributed along the junction of differentially contracting bodies. Maximum shear stress always occurs at the edge of the joint layer *i.e.* at the free edges of the BZ [14].

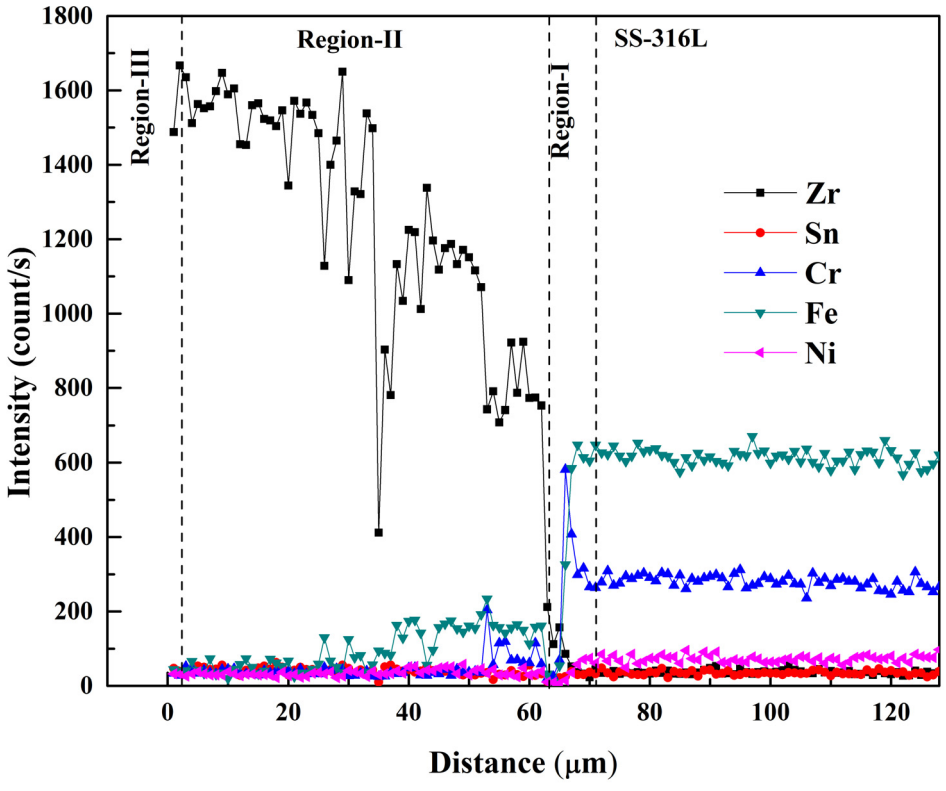

Fig. 3. The compositional line scan of BZ through EDS

TABLE 5

Mechanical properties of SS-316L, Zircaloy-4 and Zr_3Fe

Alloy	Coefficient of Thermal Expansion, α ($/^oC$)	Modulus of Elasticity, E (GPa)	Shear Modulus, G (GPa)	Poison's Ratio, υ
SS-316L	16×10^{-6}	205	82	0.280
Zircaloy-4	6×10^{-6}	99.3	36	0.370
Zr_3Fe [31]	6.1×10^{-6}	0.13	0.04	0.372

The problem under discussion has two layers, see the schematic diagram Fig. 4, Zircaloy-4 and SS-316L having uniform thickness of (t_1, t_2) with elastic moduli (E_1, E_2) and thermal coefficient of expansion (α_1, α_2), for values see Table 5. The joint (BZ) between these two layers have thickness η and shear modulus G.

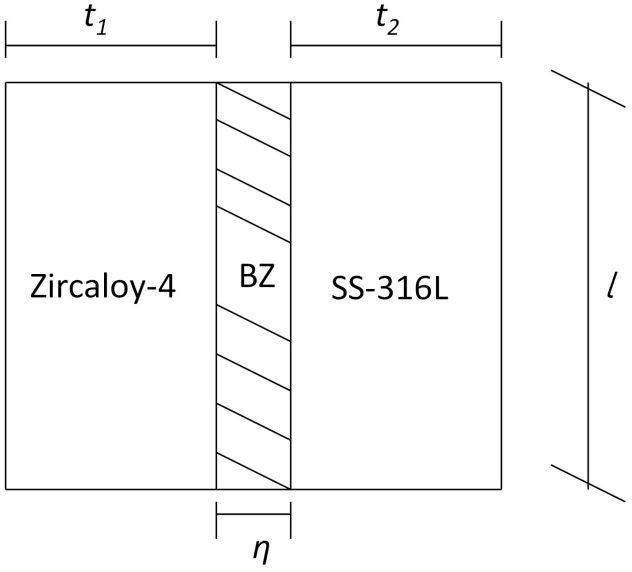

Fig. 4. The schematic diagram, illustrating base metal alloys and Bonded Zone (BZ)

Also $\eta << t_1, t_2$.

In case of completely filled joint of two elastic layers, the shear stress τ is given as; [14]

$$\tau = \frac{(\alpha 1+\alpha 2)TG\,\sinh(\beta x)}{\beta\eta\,\cosh(\beta l)} \tag{1}$$

Where:

$$\beta^2 = \frac{G}{\eta}\left(\frac{1}{E_1 t_1}+\frac{1}{E_2 t_2}\right) \tag{2}$$

Physically the shear stress is zero at the center, and increases gradually to a maximum at the free edge. The value of maximum shear stress is;

When; $x = l$, (l = length of joint)

$$\tau_{\max} = \frac{(\alpha 1+\alpha 2)TG\,\tanh(\beta l)}{\beta\eta} \tag{3}$$

Since, $\tanh(\beta l) \sim 1$

$$\tau_{\max} = \frac{(\alpha 1+\alpha 2)TG}{\beta\eta} \tag{4}$$

Maximum shear stress $\tau_{\max}$ acting on the observed brittle phase of the BZ can be calculated by applying Eq. 4.

The thickness of the BZ (η) was taken as variable to understand the effect of shear stress on cracking. The bonded zone (BZ) under discussion has a thickness ($\eta \sim 225$ μm) and comprises three regions. Distribution of island like ductile α-Zr throughout the Region-II gives it a better strength against the shear stress. The strength of Region-I calculated in terms of microhardness also lies in close proximity of SS-316L. Therefore, both of these regions (Region-I and Region-II) can be taken as the part of the SS-316 to simplify the calculations of shear stress on cracked phase. Maximum shear stress was calculated for 225, 155, 100, 50 and 10 (μm) thickness of diffusion transformed Zr_3Fe brittle phase. System under discussion was also solved for 100, 400, 600 and 800°C temperature using Eq. 4 and plotted in Fig. 5. Maximum shear stress acting on the free edge has showed an inverse relation with thickness of the BZ for a given temperature change. Increasing the thickness of BZ the shear stress acting on the free edge will be decreased but it may not serve the purpose of improving the integrity of BZ. Because larger BZ would result even larger region-III in BZ which may not withstand even lower shear stress. .Better integrity of the brazing joint can be obtained by improving the structural morphology of BZ and by impeding the diffusion of Fe into Zircaloy-4 matrix. In present study, Region-II has showed integrity with the thickness of ~62 μm. It was mainly comprised of isothermally solidified α-Zr and athermally solidified multiphase composite. The strength of BZ can be improved by increasing the relative proportion of α-Zr and multiphase composite i.e region-II. This can be achieved by introducing a thicker interlayer. Moreover, the diffusion of Fe atoms into Zircaloy-4 matrix can be controlled by optimizing the brazing time.

4. Conclusions

Bonding of dissimilar materials, Zircaloy-4 and SS-316L is possible by introducing Zr-based ($Zr_{55}Cu_{30}Al_{10}Ni_2Fe_3$-at. %) amorphous interlayer at high vacuum. Bonded Zone was found to constitute morphologically distinct two interfacial and a central regions. Cr-rich layer was formed at SS-316L interface (Region-I) of BZ and it acted as a barrier against the diffusion of Zr into the SS-316L matrix. Diffusion of Fe atoms was occurred into Zircaloy-4 matrix from the molten pool at brazing temperature. During cooling, peritectoid reaction was occurred and Fe enriched β-Zr and Zr_2Fe were transformed into brittle Zr_3Fe phase. Central region of BZ was observed to have composite structural morphology which mainly comprised of isothermally solidified α-Zr and athermally solidified intermetallic phases. Cracking was occurred in diffusion transformed brittle phase of

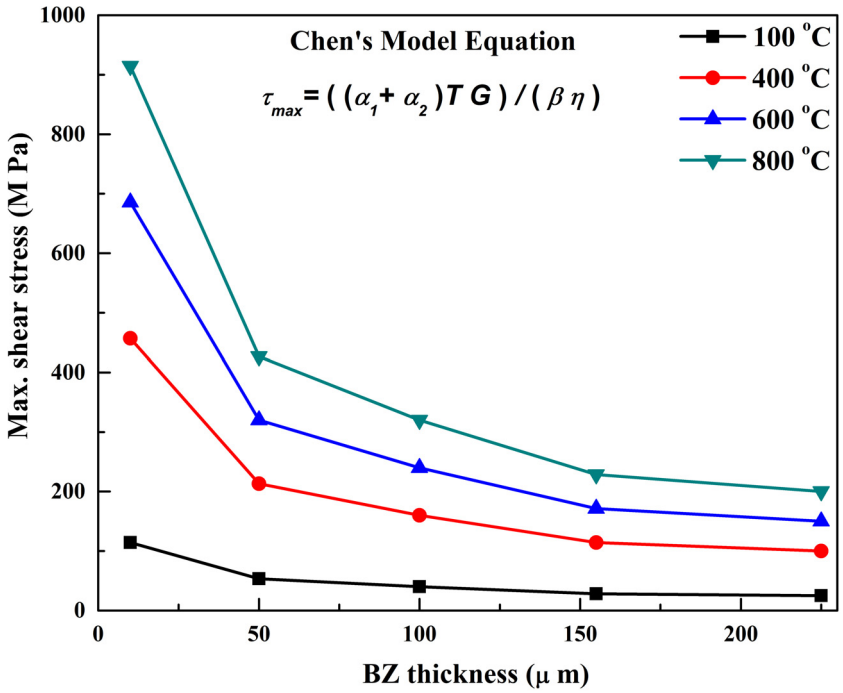

Fig. 5. Maximum shear stress behavior with varying BZ thickness and temperature

BZ in Region-III due to the shear stress. Shear stresses acting on the BZ were attributed to large difference in coefficient of thermal expansion of base alloys.

REFERENCES

[1] K. Bhanumurthy, J. Krishnan, G.B. Kale, S. Banergee, J. Nucl. Mater. **217**, 67-74 (1994).

[2] G. Perona, R. Sesini, W. Nicodemi, R. Zoja, J. Nucl. Mater.**18**, 278-291 (1966).

[3] M. Ahmad, J.I. Akhter, M. Akhar, M. Iqbal, J. Mat. Sci. **42**, 328-331 (2007).

[4] W.A. Owczarski, AWS 42th Annual Meeting 78-83, New York 1961.

[5] M. Ahmad, J.I. Akhter, M.A. Sheikh, M. Akhtar, M. Iqbal, M.A. Chaudhry, J. Nucl. Mater. **301**, 118-121 (2001).

[6] H.I. Shaaban, F.H. Hammad, J. Nucl. Mater. **71**, 277-285 (1978).

[7] H.I. Shaaban, F.H. Hammad, J. Nucl. Mater. **78**, 431-437 (1978).

[8] M.L. Wayman, R.R. Smith, M.G. Wright, Metall. Trans. A. **17A**, 429-435 (1986).

[9] M. Ahmad, J.I. Akhter, Q. Zaman, M.A. Shaikh, M. Akhtar, M. Iqbal, E. Ahmed, J. Nucl. Mater. **317**, 212-216 (2003).

[10] G.B. Kale, K. Bhanumurthy, K.C. Tatnakala, S.K. Khera, J. Nucl. Mater. **138**, 73-80 (1986).

[11] B. Akalin, V. Tfedotor, O. Nserrjukov, A.E. Plyuschev, NANCY, 142-145, FRANCE 27-29 October, (2004).

[12] M.E. Bajgholi, E. Heshmat Dehkordi, J. Adv. Mat. Proc. **1**, 51-59 (2013).

[13] M. Iqbal, J.I. Akhter, W.S. Sun, J. Z. Zhao, M. Ahmad, W. Wei, Z. Q. Hu, H. F. Zhang, Mater. Lett. **60**, 662-665 (2006).

[14] W.T. Chen, C.W. Nelson, Ibm. J. Res. Dev. **23** (2) (1979).

[15] O. Volkersen, Lufifahrtforschung. **15**, 41 (1938).

[16] X.P. Zhang, Y.W. Shi, Scripta Mater. **50**, 1003-1006 (2004).

[17] H. Nakagawa, C.H. Lee, T.H. North, Metall. Trans. A. **22A**, 543-555 (1991).

[18] W.F. Gale, D.A. Butts, Sci. Technol. Weld. Joi. **9** (4), 283-300 (2004).

[19] D. Amiri, S.A. Sajjadi, R. Bakhtiari, A. Kamyabi-Gol, J. Manuf. Process. **32**, 644-655 (2018).

[20] M. Pouranvari, A. Ekrami, A.H. Kokabi, J. Alloy. Compd. **461**, 641-647 (2008).

[21] P. Nash, C.S. Jayanth, Bull. Alloy Phase Diagrams. **5**, (2),144-148 (1984).

[22] H. Zau, G.M. Hoods, J.A. Ron, R.J. Schultz, Metall. Mater. Trans. A. **25**,1359-1365 (1994).

[23] L. Kumar, R.V. Ramnujan, R. Tewari, P. Mukhopadhyay, S. Benerjee, Scripta Mater **40** (6), 723-728 (1999).

[24] J.A. Sawicki, G.M. Hood, H. Zou, J. Nucl. Mater. **218**, 161-165 (1995).

[25] M. Ahmad, J.I. Akhter, M. Shahzad, M. Akhtar, J. Alloy Compd. **457**, 131-134 (2008).

[26] H. Uetsuka, F. Nagase, T. Otomo, J. Nucl. Mater. **246**, 180-188 (1997).

[27] P. Gr. Lucuta, I. Patru, F.Vasiliu, J. Nucl. Mater. **99**, 154-164 (1981).

[28] D. Arias, J.P. Abriata, Bull. Alloy Phase Diagram. **9** (5), 597-604 (1988).

[29] D.S. Duvall, W.A. Owezarski, D.F. Paulonis, Weld. J. **53** (4), 203-214 (1974).

[30] I. Tuah Poku, M. Doller, T. B. Massalski, Metal. Trans. A. **19**, 675-686 (1988).

[31] D. Chapelle, A. Hocine, S. Carbillet, M.L. Boubakar, Mater. Design. **36**, 459-469 (2012).